

A STATISTICAL APPROACH TO THE PREDICTION OF GASEOUS POLLUTANT DISPERSION IN THE ATMOSPHERE USING CFD

Paulo Eduardo Batista de Mello

Departamento de Engenharia Mecânica – Escola Politécnica – USP
Av. Prof. Mello Moraes, 2231, Cidade Universitária, São Paulo, SP, CEP 05509-900, Brasil.
padu@usp.br

Jurandir Itizo Yanagihara

Departamento de Engenharia Mecânica – Escola Politécnica – USP
Av. Prof. Mello Moraes, 2231, Cidade Universitária, São Paulo, SP, CEP 05509-900, Brasil.
jiy@usp.br

Abstract. The present work proposes a numerical and statistical approach, using computational fluid dynamics (cfd), for the study of atmospheric pollutant dispersion. The methodology described permits to evaluate the mean and the standard deviation of the pollutant concentration in a given calculation domain position. The PHOENICS code is used for the simulation of turbulent air flow and dispersion through a two-dimensional obstacle which simulates a hill. The $k-\varepsilon$ model adequately simulates this kind of flow, including the recirculation bubble, when C_μ constant is modified to 0.03. The numerical results for the mean concentration are in good agreement with the experimental results.

Keywords: pollutant dispersion, atmosphere, cfd, turbulence modelling, boundary layer.

1. Introduction

The prediction of the gaseous pollutant dispersion in the atmosphere requires the use of a closure model for the turbulent flow. It is known that due to the turbulence presented in the atmospheric air flow, the mean value of the pollutant concentration is an insufficient final result since, at a given moment, the instantaneous concentration value can be much more than the mean.

Turbulence modelling has been a research field in constant development. Many turbulence models are available in the literature, with variable levels of complexity. The standard $k-\varepsilon$ model and its variations are in the midway between the simple mixing length models and the more complex Reynolds stress models. Therefore these $k-\varepsilon$ models have been extensively used to solve engineering problems. The $k-\varepsilon$ model and many of its variations are implemented in PHOENICS and are among the most tested and validated turbulence models.

The CFD code PHOENICS (acronym for Parabolic Hyperbolic or Elliptic Numerical Integration Code Series) is used for the simulation of the turbulent air flow and dispersion through a two-dimensional obstacle which simulates a hill. The source of pollutant is a 10 mm diameter tube placed upwind from the hill. The experimental results of Costa et al. (1993) and Chatzipanagiotidis and Olivari (1996) were used for validation of the numerical results.

In the first experimental work, Costa et al. (1993) analyzed the effects of the upstream turbulence on the flow over hills. They produced three different upstream flows, varying turbulence intensities and distributions. They analyzed their effects on the flow, particularly over the length of the recirculation bubble that is formed downstream the hill. The two-dimensional hill has an isosceles triangular section of 136 mm base and 34 mm height. The dimensions of the wind tunnel and the position of the hill can be viewed in Fig. (1).

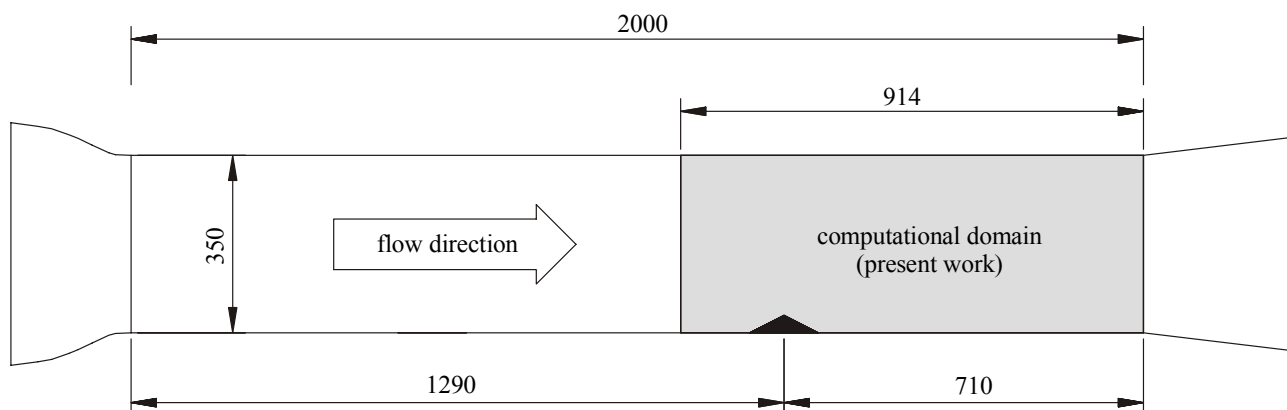


Figure 1. Wind tunnel dimensions and position of the triangular hill in the experimental work of Costa et al. (1993).

With the same experimental setup used by Costa et al. (1993), Chatzipanagiotidis and Olivari (1996) studied the dispersion from a source placed upwind from the hill. The same upstream flows of the first work were simulated, with the same three turbulence intensities and distributions. All the concentration measurements were adimensionalized by the concentration of a particular position of the wind tunnel, near the source, due to limitations imposed by the image processing technique used for these measurements. The unique data of the work of Chatzipanagiotidis and Olivari (1996) is the probability density functions for the concentration observed in some selected positions downstream of the hill. These statistical data allow to better understand the phenomena and to generate more useful information about concentration, in addition to the mean. With these new statistical data, it is possible to estimate the probability for the concentration to exceed a given limit. The objective of the present work is to obtain numerically the mean and variance of the concentration for the experimental conditions mentioned above.

2. Mathematical Model

The air flow simulated numerically in this study is governed by the Navier-Stokes and continuity equations. The Eq. (1) and Eq. (2) are Reynolds averaged conservation equations of momentum and mass for the case where the flow can be considered steady, incompressible and adiabatic

$$\frac{\partial U_i}{\partial x_i} = 0 \quad (1)$$

$$\frac{\partial}{\partial x_i} (U_i U_j) = -\frac{1}{\rho} \frac{\partial P}{\partial x_i} + \frac{\partial}{\partial x_i} \left(\nu \frac{\partial U_i}{\partial x_i} \right) + \frac{\partial}{\partial x_i} (-\overline{u'_i u'_j}) \quad (2)$$

where U is the mean velocity, u' is the velocity fluctuation, P is the mean pressure and ν is the kinematic viscosity.

Since the air flow in the present case is turbulent, the momentum equations include turbulent fluxes $-\overline{u'_i u'_j}$ which are modelled using the Boussinesq hypothesis so that Reynolds stresses can be linked to the mean rates of deformation

$$-\overline{u'_i u'_j} = \nu_t \left(\frac{\partial U_i}{\partial x_j} + \frac{\partial U_j}{\partial x_i} \right) - \frac{2}{3} k \delta_{ij} \quad \delta_{ij} = \begin{cases} 1 & \text{for } i = j \\ 0 & \text{for } i \neq j \end{cases} \quad (3)$$

where ν_t is the eddy viscosity (or turbulent viscosity), k the kinetic energy and δ_{ij} the Kronecker delta.

One turbulence model is needed for the proper eddy viscosity evaluation. Versteeg and Malalasekera (1995) present a review of the most used turbulence models, among them the well known k - ε model. The k - ε model is one of the most used and validated models since it is available in almost all CFD codes. In the PHOENICS code, used in the present work, the k - ε model and many of its variations are available. In these models the eddy viscosity ν_t is related to the turbulent kinetic energy k and its rate of dissipation ε . In the present work, the variation of the k - ε model proposed by Lam; Bremhorst (1981) is used. This k - ε variation is appropriate for the solution of the viscous sub-layer and reduces to the standard k - ε model far from the walls. The eddy viscosity is modelled by Eq.(4)

$$\nu_t = C_\mu f_\mu \frac{k^2}{\varepsilon} \quad (4)$$

where C_μ is a constant and f_μ is a wall-damping function. This damping function, as proposed by Lam and Bremhorst (1981) tends to unity far from the wall.

In the k - ε model and its variations, two additional conservation equations must be solved: one for the turbulent kinetic energy k and other for its rate of dissipation ε . These two equations, for the Lam and Bremhorst (1981) k - ε model are shown in the Eq. (5) and Eq. (6). In Eq. (5) the last two terms represents the turbulent kinetic energy rates of production and destruction, respectively. The same can be said about Eq. (6) for the kinetic energy dissipation ε

$$\frac{\partial}{\partial x_i} (U_i k) = \frac{\partial}{\partial x_i} \left(\nu + \frac{\nu_t}{\sigma_k} \frac{\partial k}{\partial x_i} \right) + P_k - \varepsilon \quad (5)$$

$$\frac{\partial}{\partial x_i} (U_i \varepsilon) = \frac{\partial}{\partial x_i} \left(\nu + \frac{\nu_t}{\sigma_\varepsilon} \frac{\partial \varepsilon}{\partial x_i} \right) + C_{1\varepsilon} f_1 \frac{\varepsilon}{k} P_k - C_{2\varepsilon} f_2 \frac{\varepsilon^2}{k} \quad (6)$$

where P_k is the rate of production of kinetic energy, f_1 and f_2 wall damping functions of the Lam and Bremhorst (1981) model, and σ_k , σ_ε , $C_{1\varepsilon}$ and $C_{2\varepsilon}$ are constants of the standard k - ε model. The rate of production of turbulent kinetic energy is calculated by Eq. (7).

$$P_k = \nu_t \frac{\partial U_i}{\partial x_j} \left(\frac{\partial U_i}{\partial x_j} + \frac{\partial U_j}{\partial x_i} \right) \quad (7)$$

The damping functions of the Lam and Bremhorst (1981) model are calculated by Eq. (8), (9) and (10). The function f_μ tends to unity far from the wall and to zero in the viscous sub-layer, so that the equation of momentum reduces to the laminar case in the region near the wall.

$$f_\mu = \left(1 - e^{-0,0165 \text{Re}_k} \right)^2 \left(1 + \frac{20,5}{\text{Re}_t} \right) \quad (8)$$

$$f_1 = 1 + \left(\frac{0,05}{f_\mu} \right)^3 \quad (9)$$

$$f_2 = 1 - e^{-\text{Re}_t^2} \quad (10)$$

where $\text{Re}_t = k^2/\varepsilon\nu$, $\text{Re}_k = k^{1/2}y/\nu$ and y is the distance to the nearest wall.

The numerical values for the empirical constants C_μ , σ_k , σ_ε , $C_{1\varepsilon}$ and $C_{2\varepsilon}$ have been obtained by data fittings for a wide range of turbulent flows. Bottema (1997) discusses the procedures used for obtaining these constants and suggests that the traditional value for the constant $C_\mu=0.09$ is overestimated for certain types of flows, in particular for the atmospheric boundary layer. According to Bottema (1997), the ‘‘thermals’’ and upstream topography present in these flows are responsible for ‘‘inactive turbulence’’, a low frequency fluctuation inefficient to promote mixing. Table (1) presents the numerical values used by the PHOENICS code for the standard k - ε and the variation proposed by Lam and Bremhorst (1981).

Table 1. Numerical values for the empirical k - ε constants used in the present work.

	C_μ	σ_k	σ_ε	$C_{1\varepsilon}$	$C_{2\varepsilon}$
standard k - ε	0.09	1.00	1.314	1.44	1.92

After the proper characterization of the flow in the domain, the three-dimensional mean concentration field can be solved separately by using Eq. (11)

$$\frac{\partial}{\partial x_i} (U_i C) = \frac{\partial}{\partial x_i} \left(D \frac{\partial C}{\partial x_i} - \overline{u'_i c'} \right) \quad (11)$$

where C is the mean concentration, c' is the fluctuation of concentration and D is the molecular diffusion.

The modelling of the last term of Eq. (11) is done by considering that the transport of the scalar C is proportional to its gradient as indicated by Eq. (12). In Eq. (12) the molecular diffusion term presented in Eq. (11) is ignored since the turbulent diffusion is predominant.

$$\frac{\partial}{\partial x_i} (U_i C) = \frac{\partial}{\partial x_i} \left(\frac{\nu_t}{\sigma_C} \frac{\partial C}{\partial x_i} \right) \quad (12)$$

Equation (13) is the equation of conservation for the variance of concentration: $\overline{c'c'}$. The variance is written as G for economy. The process of obtaining Eq. (13) from the concentration equation takes a lot of algebra. It is achieved by multiplying the conservation equation for instantaneous concentration c by twice its fluctuation c' ,

$$\frac{\partial}{\partial x_i} (U_i G) = \frac{\partial}{\partial x_i} \left(\frac{\nu_t}{\sigma_G} \frac{\partial G}{\partial x_i} \right) + 2 \frac{\nu_t}{\sigma_C} \left(\frac{\partial C}{\partial x_i} \right)^2 - 2C_G G \frac{\varepsilon}{k} \quad (13)$$

where σ_C , σ_G , C_G are constants.

3. Wind Tunnel Experiments

In the wind tunnel experiments used for validation the length dimensions are adimensionalized by the hill height $H=34\text{mm}$, the velocities by the free flow velocity $U_f=5\text{ m/s}$ and the concentration by the maximum concentration C_{max} observed at the section $x = -3H$, Fig. (2). The absolute value of C_{max} and the concentration at the source are not available. Costa et al (1993) presents vertical profiles of velocity and rms of turbulent fluctuations for the three upstream flows at sections $-6H, 0H, 4H, 9H$ and $21H$. The measurements were performed with hot wire anemometers and a two-component Laser Doppler Velocimeter. For each upstream flow the length of the recirculation formed downstream of the hill is presented, ranging from $7H$ to $11H$, depending on the upstream flow.

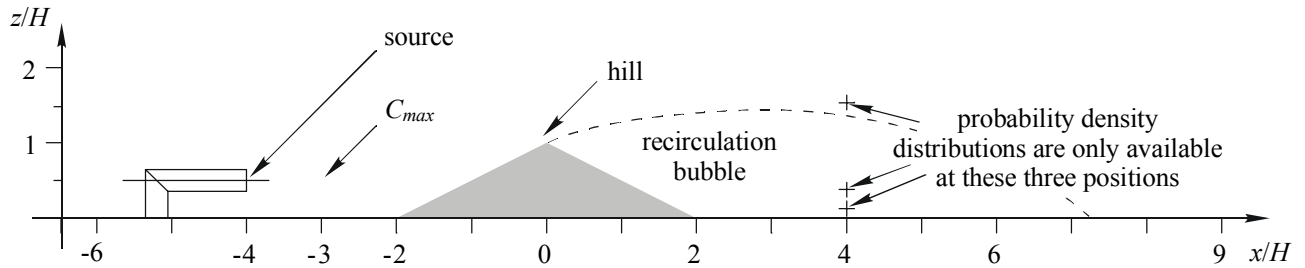


Figure 2. Measurement positions for the wind tunnel experiments of Costa et al. (1993) and Chatzipanagiotidis and Olivari (1996).

Chatzipanagiotidis and Olivari (1996) present vertical profiles of mean concentration for sections $0H, 2H, 4H$ and $9H$, but not for all the three upstream flows. Horizontal mean concentration profiles for sections $4H$ and $6H$ are also available, at the height of maximum concentration. Concentration probability density distributions are presented for three heights at position $4H$ for one of the three upstream flows: the simulated atmospheric boundary layer. The source of pollutant was a tube of inner diameter equal to 10 mm , with its exit aligned to the flow. It was placed at $z/H = 0.5$ and $x/H = -4$. The measurements were performed using light scattering technique. The plume was illuminated by a laser sheet and the scattered light was detected by two video cameras conveniently disposed.

4. Numerical Method

The PHOENICS code is based on the finite volume method. The equations of the mathematical model are integrated over each control volume of the domain, and solved numerically. The code uses a staggered grid arrangement for velocities and scalar variables. The hybrid scheme is employed for the interpolation of the convective terms when solving the flow. The second order scheme proposed by Gaskell and Lau (1988), named by the authors SMART – Sharp and Monotonic Algorithm for Realistic Transport – is used for the solution of the scalars mean and variance of the concentration.

5. Computational Grid

Since the model of Lam and Bremhorst (1981) dispenses the use of wall-functions, the flow must be solved close to the wall, in the viscous sub-layer. A minimum number of volumes must be supplied in the proximity to the wall in order to guarantee good results as the first volume close to the wall should not exceed $y^+ > 1$. This criterion would generate grids with too many volumes when using uniform disposition of the volumes. The alternative is to use geometric progressions for the disposition of volumes, as in the grid of Fig (3), where the two-dimensional grid used to solve the flow is shown. The flow was considered to be essentially two-dimensional. The influence of the wind tunnel lateral wall over the flow was not considered.

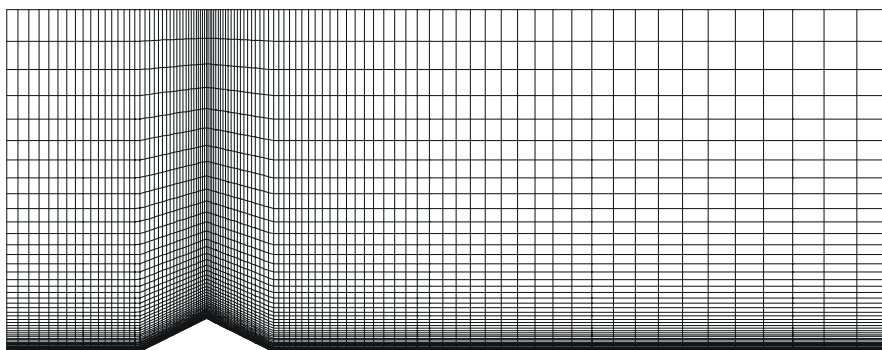


Figure 3. Two-dimensional grid showing refinement near the wall using geometric progressions.

The velocities and turbulent viscosity distributions, obtained by solving the two-dimensional flow, were interpolated to a three-dimensional grid, more suited for the dispersion solution. The three-dimensional grid was not refined close to the wall and near the hill peak, like in Fig.(3), but close to the pollutant source.

As the grid interpolation and geometric progression refinement were not available in the PHOENICS code, they were implemented by the authors.

6. Boundary Conditions

Boundary conditions must be supplied to the numerical code in all the physical boundaries of the domain. Four different types of boundary conditions were used in the present computations: inlet, outlet, walls and symmetry plane.

At the outlet the boundary condition is constituted by uniform pressure and null diffusive gradients on the flow direction. At the wind tunnel surfaces, the no slip condition requires the velocities to be zero. The turbulent kinetic energy is zero and the gradient of kinetic energy dissipation is also zero. No wall-functions were used since the low-Reynolds model of Lam and Bremhorst (1981) does not require them. At the symmetry plane the gradient of all variables are set to zero.

At the domain inlet, the velocity and turbulence vertical profiles must be conveniently provided as boundary conditions. Costa et al. (1993) proposed, in their experimental work, that the upstream mean velocity profile, at position $x/H = -6$, can be characterised by the exponent p of the power law shown in Eq. (14).

$$\frac{U}{U_{\infty}} = \left(\frac{z}{\delta}\right)^p \quad (14)$$

The three different inlet flows studied by Costa et al. (1993) can be summarized by Tab.(2), where δ is the observed boundary layer thickness and p the exponent of the power law Eq.(14).

Table 2. Exponent p and boundary layer thickness of the power law for the three different inlet flows

	upstream flows		
	N	B	G
δ (mm)	60	150	40
p	0,16	0,17	0,08

The N flow is characterized by the natural boundary layer developed at the wind tunnel surface and presents low turbulence. The B flow is a simulated atmospheric boundary layer generated with a system of vortex generators, barriers and surface roughness. The G flow is a grid generated turbulence flow. Figure (4) shows the comparison between the measured velocity profile and the fitted power law, which shows a good agreement in the boundary layer region.

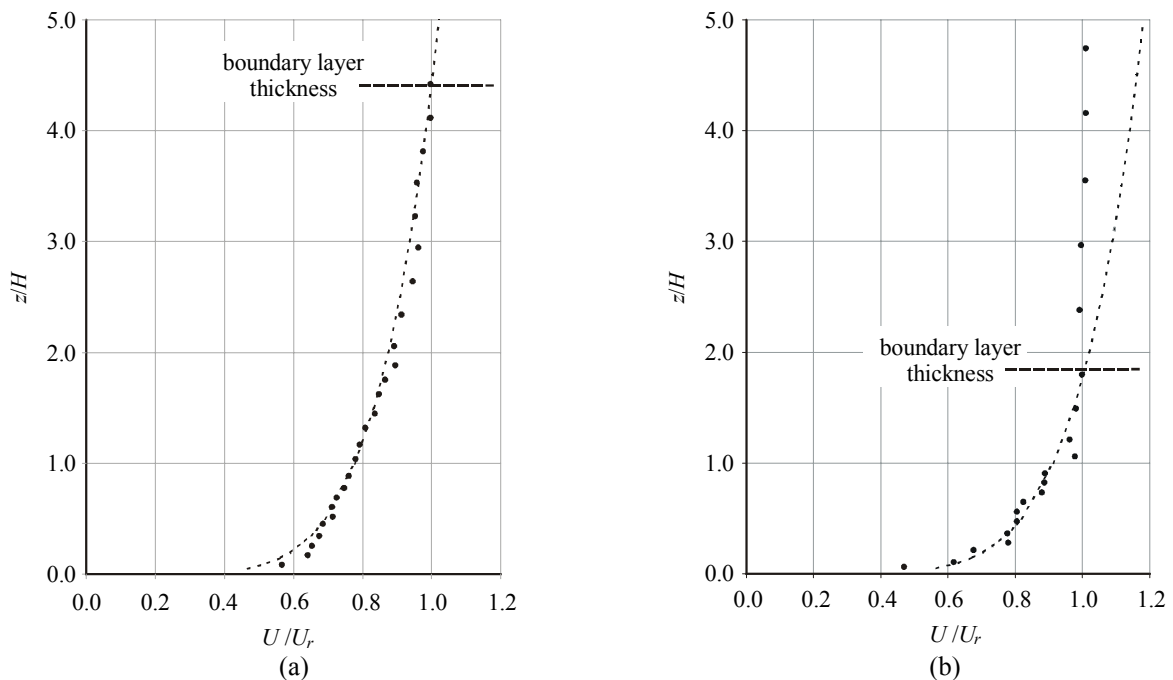


Figure 4. Agreement between measured points and the power law velocity profile proposed by Costa et al. (1993). a) B flow b) N flow.

The vertical profiles of rms of normal turbulent fluctuations can be seen in Fig. (5). They were used to obtain curve fits by least squares method, one for each component, from where the turbulent kinetic energy k can be estimated. Figure (5) shows that the polynomials represent the experimental points satisfactorily.

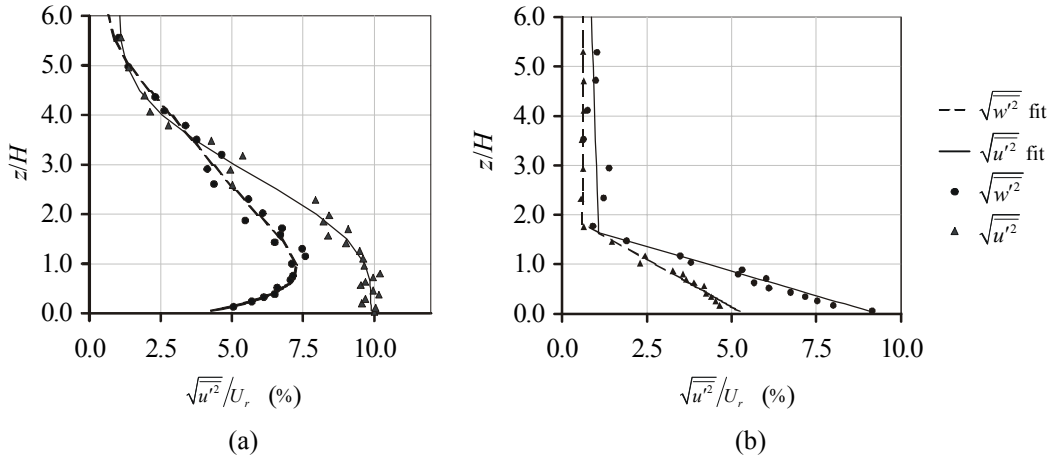


Figure 5. Vertical profiles of normal turbulent fluctuations rms. The symbols are the experimental measures of Costa et al. (1993). The lines on both graphs are the curves that fit the experimental data by least squares method. a) B flow b) N flow.

Since only two fluctuations components are presented in the experimental work of Costa et al. (1993), the turbulent kinetic energy k was approximated by Eq. (15), where the unknown component is not considered.

$$k = \frac{1}{2}(\overline{u'^2} + \overline{v'^2} + \overline{w'^2}) \quad (15)$$

The upstream vertical profile of the turbulent kinetic energy $k(z)$ obtained from the data fittings are given by Eq. (16) for the B flow and by Eq. (17) for the N flow. These vertical profiles are used as boundary conditions for the k equation and are plotted in Fig. (6).

$$k(z) = 2.379 \times 10^{-4} z^5 + 5.902 \times 10^{-3} z^4 + 5.281 \times 10^{-1} z^3 - 1.978 \times 10^{-1} z^2 + 2.186 \times 10^{-1} z^1 + 2.035 \times 10^{-1} \quad (16)$$

$$k(z) = \begin{cases} 6.056 \times 10^{-2} z^2 - 2.296 \times 10^{-1} z + 2.181 \times 10^{-1} & \text{for } z/H \leq 1.64 \\ 2.8 \times 10^{-3} & \text{for } z/H > 1.64 \end{cases} \quad (17)$$

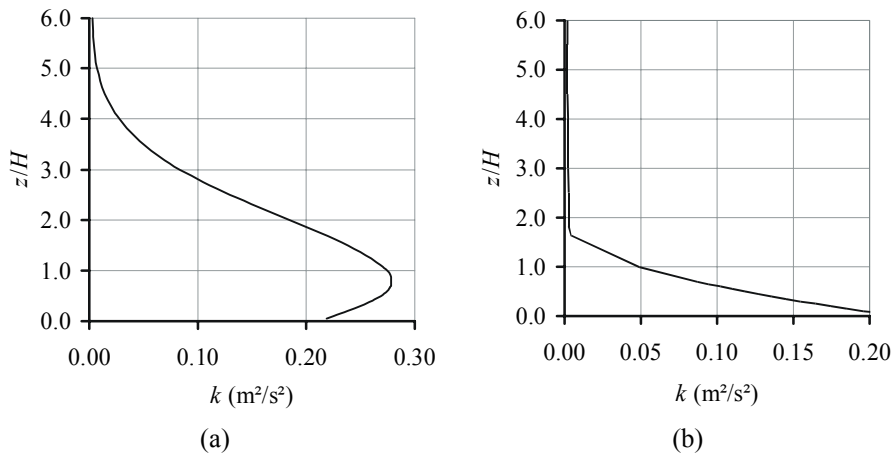


Figure 6. Vertical profiles of turbulent kinetic energy used as boundary conditions in the inlet: a) B flow; b) N flow.

The vertical profiles of kinetic energy dissipation $\epsilon(z)$ are not available in the experimental works of Costa et al (1993). These profiles were approximated by Eq. (18) from the profiles of $k(z)$.

$$\varepsilon(z) = C_{\mu}^{3/4} \frac{k^{3/2}}{\ell} \quad \ell = 0.07L \quad (18)$$

where L is a length scale of the flow, considered to be equal to the boundary layer thickness.

7. Presentation and Analysis of Results

The influence of the grid refinement on the numerical results was evaluated with numerical simulations carried out for various grid sizes. This evaluation showed that a grid with 160×70 or more volumes is adequate to provide consistent results when the recirculation bubble length formed downstream of the hill is considered.

7.1 Effect of the upstream turbulence conditions over the flow

According to Costa et al (1993), as the upstream turbulence increases, the recirculation length formed downstream of the hill decreases. In addition, this length is not influenced by the vertical distribution of the turbulence, but only its intensity observed on the upstream flow.

Table 3: Numerical results for the recirculation bubble length formed downwind of the hill. This length is considered as the position where the flow inverts its direction, at 1 mm from the wall.

Recirculation bubble length	N flow	B flow
experimental	10 to 11 H	7 to 8 H
k - ε model - $C_{\mu}=0,09$	8.9 H	4.6 H
k - ε model - $C_{\mu}=0,07$	9.8 H	5.4 H
k - ε model - $C_{\mu}=0,05$	11.1 H	6.5 H
k - ε model - $C_{\mu}=0,03$	12.9 H	8.5 H
k - ε model – Chen Kim – $C_{\mu}=0,09$	13.9 H	8.7 H

The numerical results presented in Tab.(3) confirm the observations of Costa et al (1993). It can be seen that the best results are achieved when $C_{\mu} \cong 0.04$ for the B flow – simulated atmospheric boundary layer– and $C_{\mu} \cong 0.06$ for the N flow – low turbulence flow. The influence of this k - ε constant over the results are better presented by Fig.(6). As commented earlier, observations made by Botema (1997) indicate that the value of C_{μ} is very dependant of characteristics of the particular flow, and that $C_{\mu} = 0.03$ gives better results when the flow is influenced by upstream topography and obstacles.

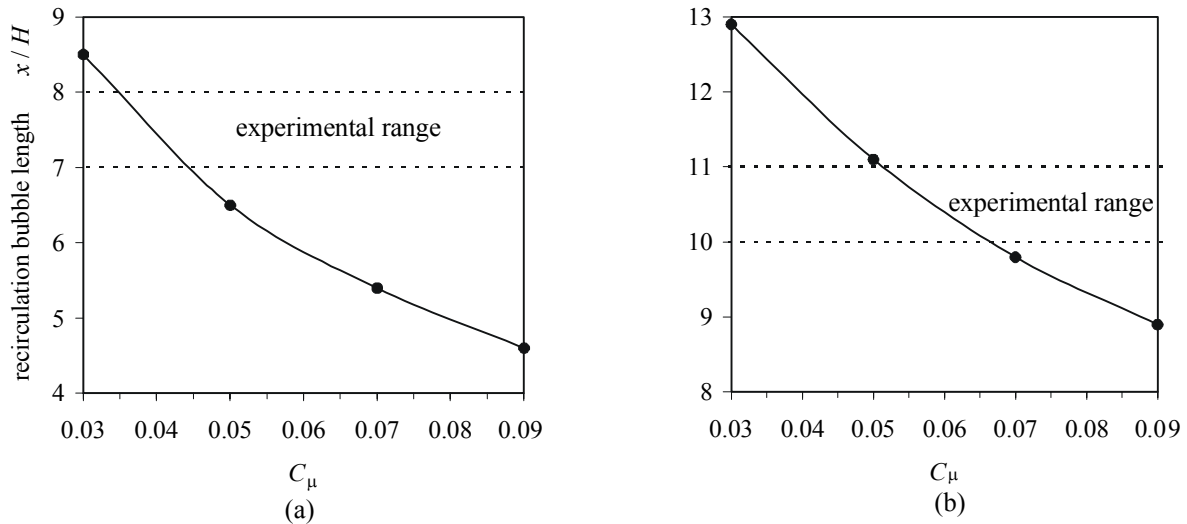


Figure 6: Recirculation bubble length obtained numerically with different values for the k - ε model C_{μ} constant. a) B flow; b) N flow.

The vertical profiles of the U velocity component in the main flow direction for the sections $0H$, $4H$ and $9H$ are presented for the B flow in Fig.(7), compared to the experimental measurements of Costa et al (1993). It can be seen that, for $C_{\mu} = 0.03$, the numerical velocity profiles are in good agreement with experimental data. Similar results were obtained for the N flow. Figure (3) shows the exact position of the sections referred by Fig.(7).

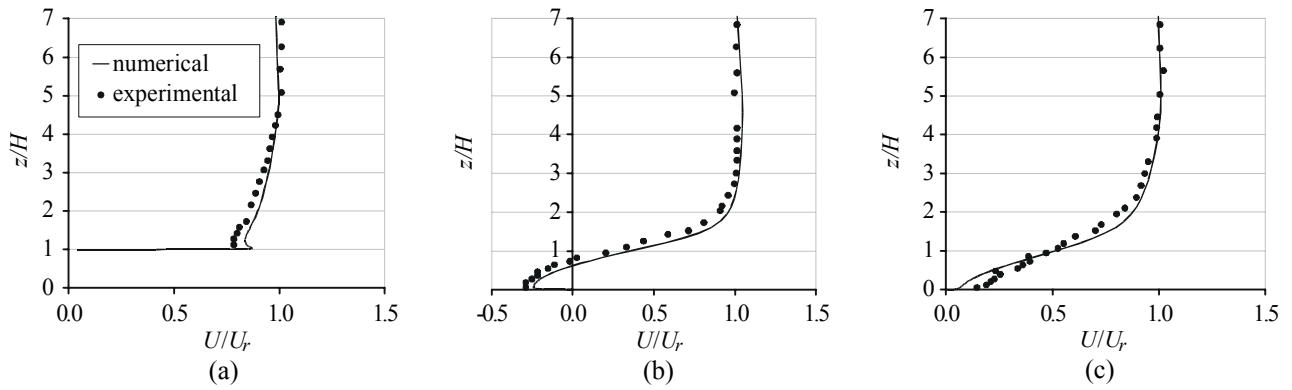


Figure 7. Comparison of the numerical vertical velocity profiles with the experimental data of Costa et al. (1993) for the B flow – simulated atmospheric boundary layer – for $C_\mu = 0.03$. a) $x = 0H$; b) $x = 4H$; c) $x = 9H$.

7.2 Dispersion results

Vertical and horizontal profiles of mean concentration can be seen in Fig.(8), for different values of σ_c . Numerical mean concentration is systematically lower than the experimental results. The reason for this disagreement is probably related to the way that experimental data were presented, by relative measurements of concentration C/C_{max} . These relative data are very dependant of the value of C_{max} . The position where C_{max} is evaluated, shown in Fig.(2), is very close to the source where the numerical approach is known to produce unsatisfactory results, as commented by Apsley (1997) and Boçon and Maliska (1997). These two numerical works report unrealistic concentration results attributed to excessive plume dispersion on the source vicinity.

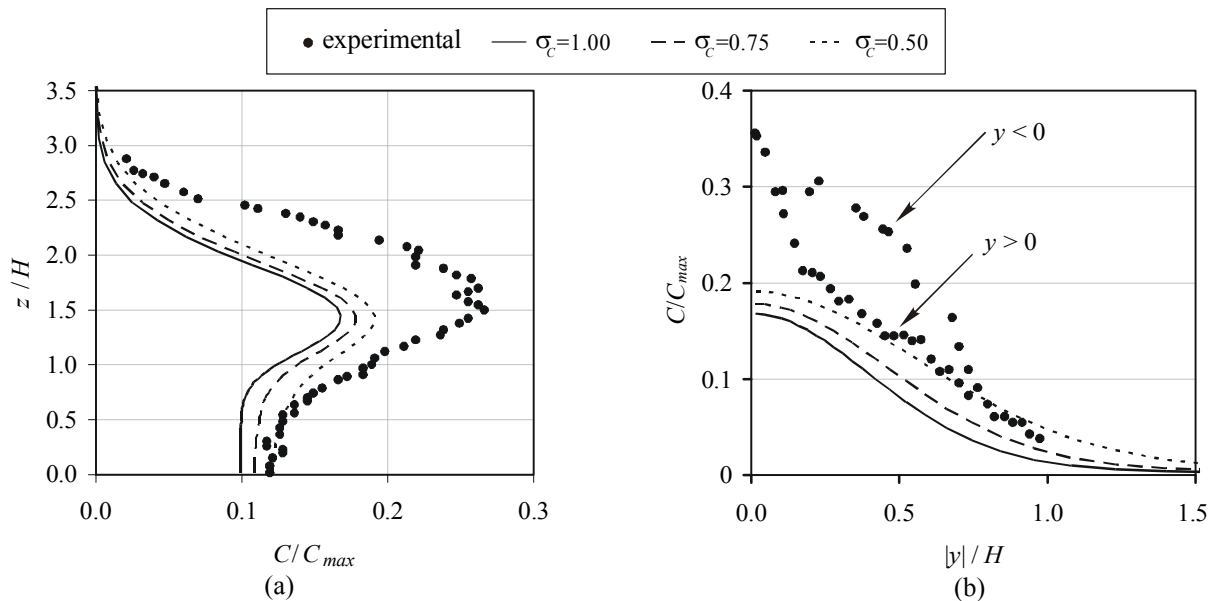


Figure 8. Comparison of the numerical concentration distributions with experimental data from Chatzipanagiotidis and Olivari (1996) for the section $x = 4H$. a) vertical distribution; b) transversal distribution where $y = 0$ is the symmetry plane of the wind tunnel.

Boçon and Maliska (1997) give a good explanation to this excessive plume spread near the source. They observed that the turbulence length scale near the source is larger than the plume dimensions. Therefore, eddies bigger than the plume could not promote the diffusion observed in the numerical results and eddy diffusivity was corrected in order to obtain more realistic dispersion. Similar corrections, as described by Boçon and Maliska (1997), are difficult to implement in the present work due to the relative nature of the measurements of concentration presented in the experimental work.

The experimental horizontal profile of mean concentration in Fig.(8b) presents unexpected asymmetry relative to the central plane of the wind tunnel and reveals the existence of experimental errors. The maximum relative concentration in the section $x=4H$ is reported to be $C/C_{max}=0.27$ by Fig.(8a) and $C/C_{max}=0.36$ by Fig.(8b), which shows some inconsistency with the experimental results, possibly due to insufficient time for the proper characterization of mean values of concentration. Anyway, the agreement between numerical and experimental results is considered

satisfactory. The differences observed are of the same order of magnitude as that observed by similar studies conducted by Apsley (1997) and Boçon and Maliska (1997).

It is important to note that, due to the mass conservation, the numerical curves in Fig.(8b) should cross each other if the concentration profiles were not relative to C_{max} . It does not occurs in Fig.(8b) since the value of C_{max} depends on the turbulent Schmidt number used in each simulation. Therefore, each curve is related to a different value of C_{max} . It was verified graphically that the horizontal profiles of Fig.(8b), obtained numerically, cross each other for absolute concentrations.

The vertical profile of standard deviation over the mean concentration, obtained by the solution of Eq. (13), is shown in Fig. (9), compared to the experimental results of Chatzipanagiotidis and Olivari (1996). The curves were obtained for $\sigma_C = \sigma_G = 0.75$. It was verified that varying the constants σ_C and σ_G did not significantly influence these results if compared to the influence of the constant C_G .

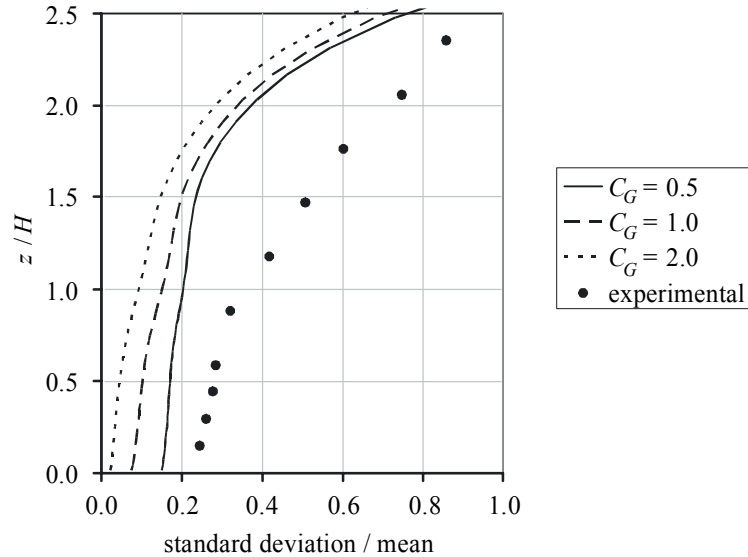


Figure 9. Comparison of the statistical parameters obtained numerically with experimental data from Chatzipanagiotidis and Olivari (1996) for the section $x = 4H$.

The experimental results for the standard deviation are available for just one section of the wind tunnel, $x = 4H$. Figure (2) shows that this particular section is located in the middle of the recirculation bubble formed downstream of the hill. Possibly, some degree of intermittency is present at this region of the flow so that the steady state assumption used in the numerical model may be inadequate. If inaccuracies are present in the mean concentration prediction, they may have a significant influence over the prediction of variance. Although the observed agreement between experimental and numerical data related to the standard deviation is only partial, more comparisons should be made in order to find the exact source of disagreement.

Chatzipanagiotidis and Olivari (1996) attempted to approximate the concentration probability density distributions obtained for positions just after the hill with the truncated beta function, but they observed that, for distances farther from the hill, the distribution tends to be Gaussian. Based on these experimental evidences, the statistical results that can be obtained with the present numerical approach could be used to estimate the probability of concentration exceed a given limit, or the fraction of the time that the concentration is above this limit. For positions far from topography influence the distribution can be considered Gaussian and the probability could be easily evaluated with the computed parameters: mean and variation of the concentration. For positions under strong influence of topography, one well known result of statistics, known as Chebyshev inequality, could be used for this purpose. Chebyshev inequality states that, for a random variable X for which its variance $\text{Var}(X)$ exists, for every number $t > 0$, Eq. (19) is valid.

$$\Pr(|X - E(X)| \geq t) \leq \frac{\text{Var}(X)}{t^2} \quad (19)$$

For $\text{Var}(X) = \sigma^2$ and $t = n\sigma$, where σ is the standard deviation, Eq.(19) states that the probability that any given random variable will differ from its mean by more than n standard deviations cannot exceed $1/n$. This probability will actually be much smaller than $1/n$ for Gaussian and beta distributions, but this upper bound cannot be made any smaller and still hold for all distributions.

8. Conclusion

Numerical simulations of air flow and dispersion were performed for obtaining statistical data in addition to the mean value of concentration in a given position. It was found that the standard value of the k - ε constant $C_{\mu}=0.03$ is more adequate for the particular problem considered, in agreement with reports found in the literature. The vertical profiles of velocity obtained numerically are very close to the experimental ones. The numerical vertical profiles of the mean concentration are in good agreement with the experimental profiles, although their numerical local values are always smaller than the experimental values. The results related to the standard deviation suggest that more comparisons with experimental work should be conducted in order to validate the proposed methodology. Finally, the presented approach is considered promising for obtaining statistical data that better describes the turbulent nature of atmospheric dispersion.

9. Acknowledgement

The authors are grateful for the support provided by CNPq (Brazilian National Research Council).

10. References

- Apsley, D.D., Castro, I.P., 1997, "Flow and dispersion over hills: Comparison between numerical predictions and experimental data", *Journal of Wind Engineering and Industrial Aerodynamics*, Vol.67, pp. 375-386.
- Boçon, F.T., Maliska, C.R., 1997, "Numerical modelling of flow and dispersion over complex terrain". 14^o COBEM – Congresso Brasileiro de Engenharia Mecânica, Anais em CDROM, Bauru.
- Bottema, M., 1997, "Turbulence closure model "constants" and the problem of "inactive" atmospheric turbulence", *Journal of Wind Engineering and Industrial Aerodynamics*, Vol. 67-68, pp. 897-908.
- Chatzipanagiotidis, A., Olivari, D., 1996, "Pollutant dispersal downstream of a hill in different wind conditions", *Journal of Wind Engineering and Industrial Aerodynamics*, Vol. 64, pp. 233-248.
- Costa, M.J., Riethmuller, M.L., Borrego, C., 1993, "Effects of upstream turbulence characteristics on the flow over two-dimensional hills", *EURASAP Int. Workshop on Wind and Water Tunnel Modelling of Atmospheric Flow and Dispersion*, Aso, Japan.
- Gaskell, P. H., LAU, A. K. C., 1988, "Curvature-compensated convective transport: SMART, a new boundedness-preserving transport algorithm", *International Journal for Numerical Methods in Fluids*, Vol. 8, pp. 617-641.
- Lam, C. K. G., Bremhorst, K., 1981, "A modified form of the k - ε model for predicting wall turbulence", *Transactions of the ASME*, Vol. 103, pp. 456-460.
- Versteeg, H.K., Malalasekera, W., 1995, *An introduction to computational fluid dynamics*, Longman Group, 257 p.